29. Gloeckler, G., Schwadron, N. A., Fisk, L. A. & Geiss, J. *Geophys. Res. Lett.* **22,** 2665–2668 (1995).
30. Fisk, L. A., Schwadron, N. A. & Gloeckler, G. *Geophys. Res. Lett.* **24,** 93–96 (1997).
31. Rucinski, D. *et al. Proc. 1st ISSI Workshop* (eds von Steiger, R., Lallement, R. & Lee, M. A.) *Space Sci. Rev.* **78,** 73–84 (1996).

Acknowledgements. The SWICS instrument was developed by a collaboration of the universities of Maryland, Bern and Braunschweig, and the Max-Planck-Institut für Aeronomie. We thank C. Gloeckler for her help with data reduction, and P. C. Frisch, E. Möbius and D. A. Gurnett for discussions. This work was supported by NASA/JPL and the Swiss National Science Foundation.

Correspondence should be addressed to G.G. (e-mail: gloeckler@umdsp.umd.edu).

Storage of hydrogen in single-walled carbon nanotubes

A. C. Dillon*, K. M. Jones*, T. A. Bekkedahl*, C. H. Kiang†, D. S. Bethune† & M. J. Heben*

* *National Renewable Energy Laboratory, 1617 Cole Boulevard, Golden, Colorado 80401-3393, USA*
† *IBM Research Division, Almaden Research Center, 650 Harry Road, San Jose, California 95120-6099, USA*

Pores of molecular dimensions can adsorb large quantities of gases owing to the enhanced density of the adsorbed material inside the pores[1], a consequence of the attractive potential of the pore walls. Pederson and Broughton have suggested[2] that carbon nanotubes, which have diameters of typically a few nanometres, should be able to draw up liquids by capillarity, and this effect has been seen for low-surface-tension liquids in large-diameter, multi-walled nanotubes[3]. Here we show that a gas can condense to high density inside narrow, single-walled nanotubes (SWNTs). Temperature-programmed desorption spectrosocopy shows that hydrogen will condense inside SWNTs under conditions that do not induce adsorption within a standard mesoporous activated carbon. The very high hydrogen uptake in these materials suggests that they might be effective as a hydrogen-storage material for fuel-cell electric vehicles.

Soots containing SWNTs were synthesized by co-evaporation of cobalt and graphite in an electric arc[4]. Amorphous carbon-coated fibres several micrometres in length were observed in the soots by transmission electron microscopy (TEM). Fibres typically consisted of 7–14 bundled SWNTs which were individually ~12 Å in diameter[5]. Cobalt nanoparticles, 5–50 nm in diameter, were also present, embedded in amorphous carbon. Electron microprobe analysis measured cobalt contents of ~20 wt%. The remainder of each sample consisted of amorphous carbon and planar graphitic fractions. Activated carbon (AC) was prepared from pitch precursors, activated by KOH, and exhibited a narrow peak in the pore-volume distribution of 30 Å with a full-width at half-maximum of ~20 Å. (Material and pore analysis was supplied by Spectracorp Ltd.) Extensive TEM examinations showed the AC to be similar in structure and overall morphology to the arc-generated soots except for the absence of SWNTs and cobalt nanoparticles.

The adsorption of H_2 on SWNT soots and AC was probed with temperature programmed desorption (TPD) spectroscopy in an ultra-high-vacuum chamber equipped with a liquid-nitrogen-cooled cryostat and a mass spectrometer. Samples weighing ~1 mg were contained in a platinum foil packet with pinholes for gas diffusion. The packet temperature was measured with a thermocouple and controlled by resistive heating. TPD experiments were performed at 1 K s^{-1}, and standard H_2 exposures were carried out at 300 torr for 10 minutes at 273 K followed by 3 minutes at 133 K except where noted. The samples were cooled to 90 K while the chamber was evacuated to $< 5 \times 10^{-8}$ torr before TPD.

H_2 desorbs from as-prepared SWNT soots (Fig. 1a) and AC (Fig. 1b) within the same temperature range, but with differing intensities. The signals are peaked just above 133 K because the H_2 pressure was reduced as the sample was cooled from 133 K to 90 K. Planar graphite cannot stabilize H_2 under these exposure conditions[5], so desorption must be from nanoporous environments[6] associated with the high-surface-area amorphous carbon fractions present in both materials. The signal from the SWNT samples (Fig. 1a) is ~10 times as great as the signal from AC (Fig. 1b), consistent with the higher amorphous carbon content (as

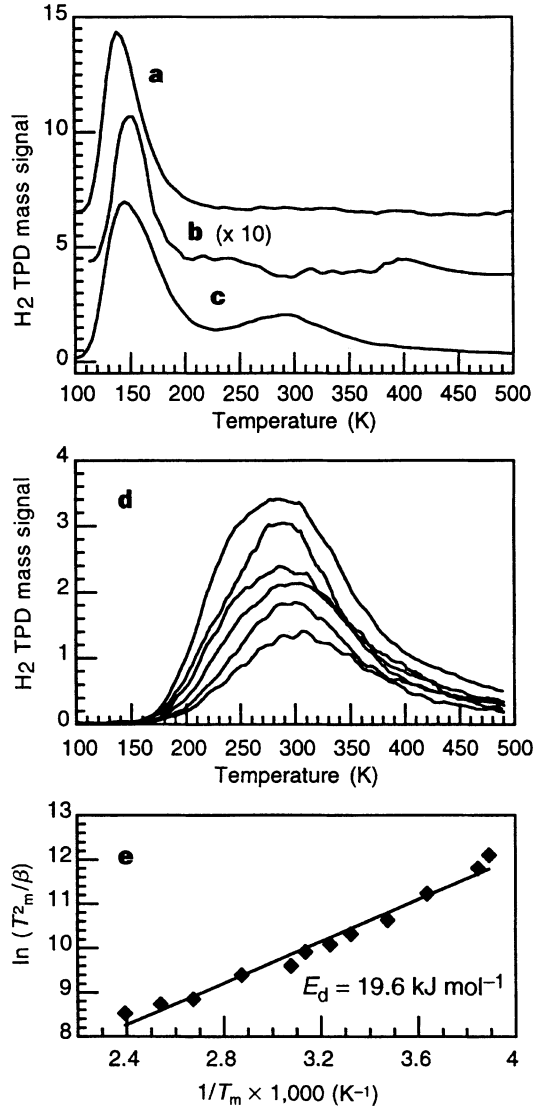

Figure 1 Temperature programmed desorption data. **a**, TPD spectrum from as-produced SWNT sample after standard hydrogen exposure. **b**, TPD spectrum from activated carbon sample, magnified 10 times, after standard hydrogen exposure. **c**, TPD spectrum from SWNT sample after heating in vacuum to 970 K and standard hydrogen exposure. **d**, Hydrogen desorption signals after exposures that populated only the high-temperature sites. Coverages range from 0.3 to saturation. **e**, Plot of $\ln(T_m^2/\beta)$ against $1/T_m$ with β varying from 0.3 to 30 K s^{-1}. The activation energy for desorption, E_d, is the slope of the line (19.6 kJ mol^{-1}).

observed by TEM) in SWNT samples. Storage of H_2 on AC materials at temperatures below 150 K has been investigated before[7] but is unattractive because cooled compressed gas containers perform equally well with or without the adsorbent[7,8]. We note that all TPD peaks presented here vary by ±20% in height and ±5° in position from sample to sample, but are highly reproducible from run to run on a given sample.

A high-temperature TPD peak representing a population of structurally unique sites is found at 288 K after SWNT soots are heated in vacuum to 970 K at 1 K s^{-1} (Fig. 1c). The adsorbed H_2 is stable at 223 K while in contact with vacuum and does not redistribute to other sites during evacuation or cooling. Figure 1d shows the TPD spectra when the high-temperature sites were selectively populated by evacuating the chamber with a sample temperature of 223 K after a 10-minute H_2 exposure at 273 K. Variation of the hydrogen pressure between 25 and 300 torr produced coverages between ~0.3 and saturation. The shift in peak temperature from 299 to 285 K with decreasing coverage is explained by first-order desorption of physisorbed H_2 with either coverage-dependent desorption energies[9] or equilibrium readsorption[10]. Shifts of 100 K or more are expected for the second-order desorption kinetics which would characterize the desorption of chemisorbed H_2 (ref. 9). First-order desorption is described by $\ln(T_m^2/\beta) = E_d/RT_m$ where T_m is the temperature at the peak maximum, E_d is the desorption activation energy, β is the heating rate and R is the universal gas constant[9]. T_m was measured for β between 0.3 and 30 K s^{-1} after only the high-temperature sites were populated at 300 torr. A plot of $\ln(T_m^2/\beta)$ against $1/T_m$ yields a straight line (Fig. 1e), confirming that H_2 is physisorbed in the high-temperature sites. The desorption activation energy, which is equivalent to the heat of adsorption in the case of physisorption[9], is 19.6 kJ mol^{-1}.

The strongly bound physisorbed H_2 that we observe is consistent with adsorption within the cavities of SWNTs[1,2,11], indicating that the tube interiors become accessible after heating in vacuum. Multiwall carbon nanotubes are opened by reaction with either O_2 (ref. 12) or CO_2 (ref. 13) because of the local strain and incorporated pentagons in the tube caps. The caps of small-diameter SWNTs should be susceptible to oxidation for the same reasons. Infrared absorption and mass spectroscopies show H_2O and CO_2 are generated by the decomposition of surface groups upon heating in vacuum. The production of H_2O and CO_2 decreases at temperatures approaching 700 K while CO generation increases. Although it is difficult to observe by TEM, we believe that surface carbon and SWNT caps are removed during this process. Arguably, heating in vacuum may simply produce a clean substrate for subsequent H_2 adsorption. However, H_2 uptake can be increased by a factor of ~3 after gentle oxidation with 1 torr H_2O. Reactive carbonaceous fractions are converted primarily to CO during the oxidation process, and additional SWNTs are evidently opened while the sample weight is decreased to ~1/3 of its initial value. Unfortunately, the degree to which SWNTs can be purified with this approach by removing amorphous carbon is limited, as SWNTs are also consumed with further oxidation. It is important to note that high-temperature desorption of H_2 is never observed from AC samples, or from arc-generated soots produced without the cobalt catalyst (which therefore contain no SWNTs).

The cobalt nanoparticles must also be considered as a possible source for the high-temperature H_2 desorption. However, H_2 TPD studies on pure cobalt single crystals[14] and polycrystalline samples[15] find TPD peaks at different temperatures, and observe second-order desorption kinetics characterizing recombinative desorption of chemisorbed H_2 (refs 14, 15). Furthermore, the amount of H_2 observed during TPD is inconsistent with either a cobalt surface or bulk hydride. Electron diffraction of cobalt nanoparticles in SWNT soots show face-centred-cubic patterns[4] initially, and a blurred superposition of hexagonal Co_3O_4 and cobalt patterns after heating in vacuum. The composite pattern is expected for cobalt metal particles covered with a thin oxide, and this coating may explain the lack of H_2 uptake by the cobalt nanoparticles.

SWNTs are the only other component unique to the soots, and are apparently responsible for stabilizing H_2 by physisorption at unusually high temperatures. Planar graphite adsorbs a complete monolayer of H_2 with a constant isosteric heat of adsorption of ~4 kJ mol^{-1} (ref. 5). Heats as high as 12 kJ mol^{-1} have been observed with certain ACs at very low coverages, but decrease to ~4 kJ mol^{-1} at higher coverages[7]. Nanometre-sized pores with high binding energies for H_2 are evidently present in AC, but constitute only a small fraction of the total porous volume. The energy of 19.6 kJ mol^{-1} measured with SWNT materials is evidence for H_2 localized in the small diameter tubes[1,2,11]. The high-temperature sites cannot be occupied in 10 minutes at 133 K as expected for slow diffusion along the internal SWNT surfaces.

The amount of H_2 adsorbed in the high-temperature peak for a sample that had been progressively oxidized in H_2O was ~0.01 wt%. Graphical integration methods applied to TEM micrographs of this sample indicated a SWNT density ranging from 0.1 to 0.2 wt% depending on the average number of tubes estimated per bundle (7 or 14, respectively). Thus, the gravimetric storage density per SWNT ranges from ~5 to 10 wt%. These values are 2.5 to 5 times greater than expected for filling tubes with close-packed H_2 at a nearest-neighbour distance of 3.51 Å (ref. 16), and a closest approach to the tube wall of 2.95 Å (ref. 5). The difference may be rationalized if SWNTs were depleted on the TEM sample grids relative to their density in the soots. Alternatively, H_2 could be packed within the tubes at higher density than assumed if H_2–H_2 repulsive interactions were screened[2,16], or additional H_2 might be

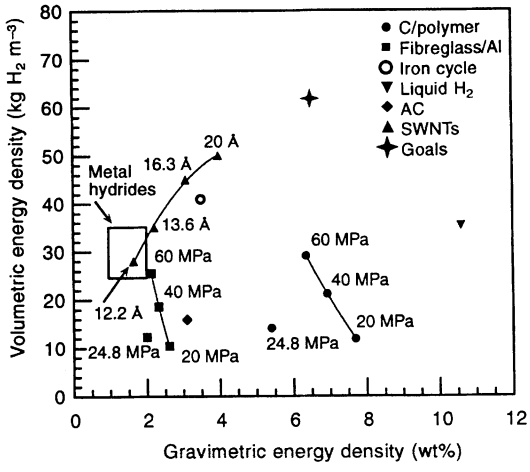

Figure 2 Installed energy densities for several vehicular hydrogen storage technologies. Lines on the plot are a guide to the eye. Calculations[21] for carbon/polymer and fibreglass/aluminium cylinders at 20, 40 and 60 MPa used performance factors of 3.5×10^5 and 1.1×10^5 m^2 s^{-2}, a ratio of outer/inner volume of 1.2 and 1.4, respectively, and a burst pressure three times the operating pressure. Data at 24.8 MPa are for currently manufactured containers (Structural Composites Industries and EDO Corporation). Required brackets and pressure regulators are not included. The area for metal hydrides encloses representative data[18,19] and considers the system weight and volume for both low- and high-dissociation-temperature materials. Data for liquid H_2 are from ref. 17, and those for adsorption on activated carbon at 155 K and 6.9 MPa are from ref. 7. The iron cycle uses on-board H_2O to generate H_2 by reaction with Fe, and requires Fe_3O_4 to be reduced to Fe off the vehicle[19]. The SWNT data are predicted for individual tubes assembled into hexagonally packed bundles assuming H_2 packing as described in the text. The points are labelled with diameters which, from smallest to largest, correspond to (9,9), (10,10), (12,12), and (15,15) 'armchair' tubes[22]. A low-pressure container with a weight equal to the SWNT weight divided by 3.5, and an outer volume 1.075 times the inner volume, is included.

adsorbed by the exterior surfaces of SWNTs and/or the interstitial spaces between bundled tubes.

A vehicle powered by a fuel cell would require ~3.1 kg of H_2 for a 500 km range[17]. This amount of H_2 stored in the weight and volume of a typical petrol tank requires system densities approaching 6.5 wt% and 62 kg H_2 m^{-3} (ref. 17). Figure 2 shows that no storage technology is currently capable of meeting these goals. SWNTs with diameters of 16.3 Å and 20 Å would come close to the target densities and operate near room temperatures if modest H_2 over-pressures compensated for the lower heats of adsorption expected in the larger cavities. These materials would have high energy storage efficiencies as they would operate at or near ambient temperatures and pressures. In contrast, 25 to 45% of the energy content in liquefied H_2 is required for liquefaction[18], and ~9% of the stored energy is needed for compression of H_2 to 20 MPa (ref. 17). For catalytic generation of H_2 by the reaction of H_2O with iron, temperatures in excess of 250 °C are required[17,19].

The effect of hydrogen over-pressure on the stability of adsorbed H_2 has not yet been investigated and remains an important question. The high-purity 13.8-Å diameter SWNT samples that have recently been produced by laser vaporization[20] should be interesting candidates for evaluation. The temperature and pressure requirements for H_2 adsorption and desorption, and the kinetics for charging and discharging, are expected to be a function of nanotube diameter and aspect ratio. Control of these parameters coupled with improvements in production, purification and alignment of SWNTs may lead to a new H_2 storage technology for hydrogen-fuelled vehicles with superior performance to currently available options. □

Received 4 November 1996; accepted 10 February 1997.

1. Gregg, S. J. & Sing, K. S. W. *Adsorption, Surface Area and Porosity* (Academic, London, 1982).
2. Pederson, M. R. & Broughton, J. Q. Nanocapillarity in fullerene tubules. *Phys. Rev. Lett.* **69,** 2689–2692 (1992).
3. Dujardin, E., Ebbesen, T. W., Hiura, H. & Tanigaki, K. Capillarity and wetting of carbon nanotubes. *Science* **265,** 1850–1852 (1994).
4. Bethune, D. S. *et al.* Cobalt-catalysed growth of carbon nanotubes with single-atomic-layer walls. *Nature* **363,** 605–607 (1993).
5. Pace, E. L. & Siebert, A. R. Heat of adsorption of parahydrogen and orthodeuterium on graphon. *J. Phys. Chem.* **63,** 1398–1400 (1959).
6. Bandosz, T. J., Jagiello, J., Amankwah, K. A. G. & Schwarz, J. A. Chemical and structural properties of clay minerals modified by inorganic and organic material. *Clay Miner.* **27,** 435–444 (1992).
7. Schwarz, J. A. *Final Report for the Tasks XC-1-1108-1 and XAE-3-13346-01* (National Renewable Energy Laboratory, Golden, Colorado, 1994).
8. Dillon, A. C., Bekkedahl, T. A., Cahill, A. E., Jones, K. M. & Heben, M. J. Carbon nanotube materials for hydrogen storage. *Proc. 1995 U.S. DOE Hydrogen Program Review* 521–541 (National Renewable Energy Laboratory, Golden, Colorado, 1995).
9. Madix, R. J. The application of flash desorption spectroscopy to chemical reactions on surfaces: Temperature programmed reaction spectroscopy. *Chemistry and Physics of Solid Surfaces* (ed. Vanselov, R.) 63–72 (CRC, Boca Raton, 1979).
10. Ibok, E. E. & Ollis, D. F. Temperature programmed desorption from porous catalysts: Shape index analysis. *J. Catal.* **66,** 391–400 (1980).
11. Peterson, B. K. & Gubbins, K. E. Phase transitions in a cylindrical pore: Grand canonical Monte Carlo, mean field theory, and the Kelvin equation. *Molec. Phys.* **62,** 215–226 (1987).
12. Ajayan, P. M. *et al.* Opening carbon nanotubes with oxygen and implications for filling. *Nature* **362,** 522–525 (1993).
13. Tsang, S. C., Harris, P. J. F. & Green, M. L. H. Thinning and opening of carbon nanotubes by oxidation using carbon dioxide. *Nature* **362,** 520–522 (1993).
14. Ernst, K. H., Schwarz, E. & Christmann, K. The interaction of hydrogen with a cobalt (1010) surface. *J. Chem. Phys.* **101,** 5388–5401 (1994).
15. Lisowski, W. The kinetics of the low-temperature hydrogen interaction with polycrystalline cobalt films. *Appl. Surf. Sci.* **37,** 272–282 (1989).
16. Nielsen, M., McTague, J. P. & Ellenson, W. Adsorbed layers of D_2, H_2, O_2, and ^3He on graphite studied by neutron scattering. *J. Phys.* **38,** C4/10–C4/18 (1977).
17. DeLuchi, M. *Hydrogen Fuel-Cell Vehicles* (Institute of Transportation Studies, Univ. California, Davis, 1992).
18. DeLuchi, M. A. Hydrogen vehicles: An evaluation of fuel storage, performance, safety, environmental impacts, and cost. *Int. J. Hydrogen Energy* **14,** 81–130 (1989).
19. T-Raissi, A. & Sadhu, A. Systems study of metal hydride storage requirements. *Proc. 1994 DOE/NREL Hydrogen Program Review* 85–106 (National Renewable Energy Laboratory, Golden, Colorado, 1994).
20. Thess, A. *et al.* Crystalline ropes of metallic carbon nanotubes. *Science* **273,** 483–487 (1996).
21. Gordon, R. Composite pressure vessels for gaseous hydrogen-powered vehicles. *Hydrogen Energy Progress V* (eds Veziroglu, T. N. Taylor, J. B.) 1225–1236 (Pergamon, New York, 1984).
22. Dresselhaus, M. S., Dresselhaus, G. & Saito, R. C_{60} related tubules. *Solid State Commun.* **84,** 201–205 (1992).

Acknowledgements. We thank Jeremy Broughton, J. Karl Johnson and Al Czanderna for technical discussions. We also thank Spectracorp Limited for activated carbon samples, and A. Mason for microprobe measurements. This work was funded by the US Department of Energy Hydrogen Program.

Correspondence and requests for materials should be addressed to M.J.H. (e-mail: mikeh@nrel.gov).

Spontaneous stratification in granular mixtures

Hernán A. Makse*, Shlomo Havlin*†, Peter R. King‡ & H. Eugene Stanley*

* *Center for Polymer Studies and Physics Department, Boston University, Boston, Massachusetts 02215, USA*

† *Minerva Center and Department of Physics, Bar-Ilan University, Ramat Gan, Israel*

‡ *BP Exploration Operating Company Ltd, Sunbury-on-Thames, Middlesex, TW16 7LN, UK*

Granular materials[1–5] segregate according to grain size when exposed to periodic perturbations such as vibrations[6–12]. Moreover, mixtures of grains of different sizes can also spontaneously segregate in the absence of external perturbations: when such a mixture is simply poured onto a pile, the large grains are more likely to be found near the base, while the small grains are more likely to be near the top[13–20]. Here we report another size-separation effect, which arises when we pour a granular mixture between two vertical plates: the mixture spontaneously stratifies into alternating layers of small and large grains whenever the large grains have larger angle of repose than the small grains. We find only spontaneous segregation, without stratification, when the large grains have smaller angle of repose than the small grains. The stratification is related to the occurrence of avalanches: during each avalanche, the grains separate into a pair of static layers, with the small grains forming a sublayer underneath the layer of large grains.

Our experimental system consists of a vertical 'quasi-two-dimensional' cell with a gap of 5 mm separating two transparent plates (made of Plexiglass or glass) measuring 300 mm × 200 mm (Fig. 1a). To avoid the effects of electrostatic interactions between the grains and the wall, the wall is cleaned with an antistatic cleaner.

In a first series of experiments, we closed the left edge of the cell leaving the right edge free, and we poured, near the left edge, an equal-volume mixture of white glass beads (mean size 0.27 mm, spherical shape, repose angle 26°), and red sugar crystals (typical size 0.8 mm, cubic shape, repose angle 39°). Figure 1a shows the result of the first series of experiments. We note two features: (1) Spontaneous stratification. We see the formation of alternating layers consisting of small and large grains—with a 'wavelength' of ~1.2 cm. (2) Spontaneous segregation. We find that the smaller grains segregate near the left edge and the larger grains segregate furthest from it and near the base[13–20].

In a second series of experiments, we confirmed the results of these initial experiments by testing for stratification and segregation using a mixture of grains of same density, consisting of fine sand (typical size 0.4 mm) and coarse sand (typical size 1 mm), suggesting that the density of the grains may not play an important role in stratification.

In all the above experiments we used mixtures composed of two types of grain with different shape, and therefore with different angles of repose. In particular we obtained stratification (plus segregation) when we used larger cubic grains and smaller spherical grains: the angle of repose of the large species was then larger than the angle of repose of the small species. Otherwise we obtained only segregation and not stratification when the large grains were less faceted than the small grains, that is, the large grains had smaller angle of repose than the small grains.

To confirm this, we performed a series of experiments using mixtures of irregular shaped sand grains (repose angle 35°, mean size 0.3 mm), and spherical glass beads (repose angle 26° smaller than the repose angle of the sand grains). We found that stratification